

## Measuring Arctic Nearshore Properties with a Multi-Frequency Airborne Electromagnetic Sensor

*Scott Holladay*  
Geosensors Inc.,  
Toronto, Ontario, Canada

*Simon Prinsenber*  
*Ingrid Peterson*  
Bedford Institute of Oceanography, Department of Fisheries & Oceans,  
Dartmouth, Nova Scotia, Canada

### ABSTRACT

Since 2001, personnel of the Bedford Institute of Oceanography have used a helicopter-mounted EM/laser system called “IcePic” to monitor the thickness and roughness of sea ice along extended survey tracks, primarily to enhance the quality of ice charts produced daily by the Canadian Ice Service. Since CIS required near-real-time results, data transmitted to CIS during surveys used the real-time output of the system, with minimal handling of the data. While in-flight data quality is high for a wide range of ice types due to joint real-time inversion of its four-frequency electromagnetic (EM) induction and laser altimeter data, further enhancements to output specifications and additional types of information can be obtained through post-flight processing, which can be performed on conclusion of a flight or while refueling. Additional parameters and capabilities that have been provided through post-flight processing include: estimates of bulk sea ice conductivity; bulk ocean surface layer conductivity; discrimination of grounded ice from ice bonded to frozen sediments; and, in shallow, low-salinity environments such as deltas, mapping of freshwater ponded beneath ice and estimation of ice/freshwater layer thickness over seawater or conductive sediments.

**KEY WORDS:** sea ice thickness; helicopter-borne sensor; electromagnetic data; electromagnetic sensor; real-time data; Canadian Beaufort Sea; Mackenzie Delta

### INTRODUCTION

Melting of the polar ice caps due to climate change has transitioned from a prediction to an accepted observation (ACIA, 2004, 2005 and IPCC, 2007). Ice extents experienced all time lows in 2007 and 2008, as documented by comparison to the last 30 years of satellite imagery (National Snow and Ice Data Centre, [www://nsidc.org](http://www/nsidc.org)). Ice thickness, an equally important ice parameter determining icepack volumes and strength, must be measured by other means. Upward-looking sonars deployed on submarines (Wadhams, 2000) and moorings (Melling et al., 2005) have estimated ice thickness through draft measurements in

the Arctic basin, while helicopter-borne electromagnetic sensors (Prinsenber et al. (1996) Peterson et al. (2008) and Haas et al. (2006) have been increasingly used to obtain ice thickness profiles in many areas. One of these helicopter-borne systems, known as IcePic (Fig. 1), acquires a multi-frequency (1.7, 5.0, 11.7, 35.2 kHz) electromagnetic and laser altimetry dataset at low (~5m) survey altitudes: in addition to ice thickness, these data can be processed to yield a variety of other ice and oceanographic parameters. This paper describes the application of these enhanced processing techniques to survey results acquired in the Mackenzie Delta in April-May 2004 as part of a larger survey, based from the CCGS *Amundsen* at its overwintering site in Franklin Bay, NWT, using a refueling site at the Tuktoyaktuk town site (Fig. 2).

### The IcePic™ Sensor System

The IcePic system comprises a nose-mounted pod enclosing a multi-frequency electromagnetic sensor, a high-precision (0.01m) laser altimeter, a 12-channel GPS receiver and a pair of tilt sensors, coupled to a data acquisition and real-time processing console inside the helicopter. The console uses Marquardt-Levinson inversion of EM-Laser data in real time at four frequencies to estimate snow plus ice thickness and bulk conductivity. The nominal thickness accuracy of the system is  $\pm 0.1\text{m}$  over smooth, level ice at 5m or lower altitude (Peterson et al., 2008), although higher accuracies are often achieved. The sensor can also be deployed on Bell 206L helicopters using a different mounting arrangement.



Fig. 1: The IcePic™ sea ice measurement system mounted on a Canadian Coast Guard BO105 helicopter.

## Study Area

The ice chart in Fig. 2 shows the land-fast ice (area F) consisting of thick first year ice and a trace of old ice in Mackenzie Delta and Franklin Bay where the icebreaker, CCGS Amundsen, over-wintered in 2003-2004. The mobile pack ice off the Mackenzie Delta consisted of 9+ tenths ice concentration of thick first year ice (>120cm).

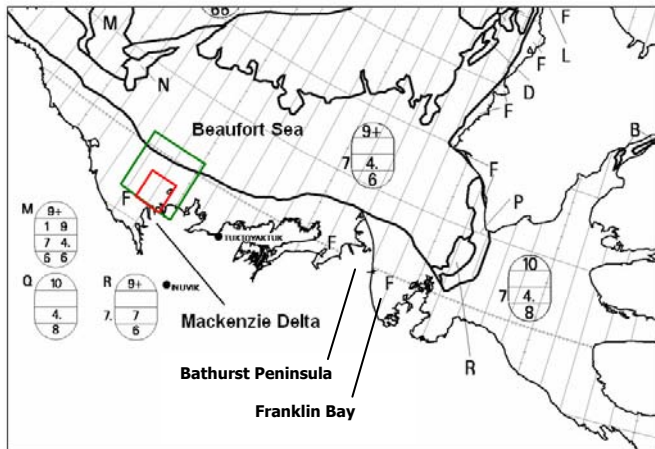


Fig. 2: Beaufort Sea ice chart for May 1, 2004, produced by the Canadian Ice Service, annotated to show study area. The small square indicates the coverage area for Fig. 9 below, while the larger square shows coverage for Fig. 10.

The surveys were designed for airborne reconnaissance of multiple areas of interest, rather than a detailed study of a particular site. They were flown from the *Amundsen*, with profiles extending around Cape Bathurst and the Tuktoyaktuk Peninsula.

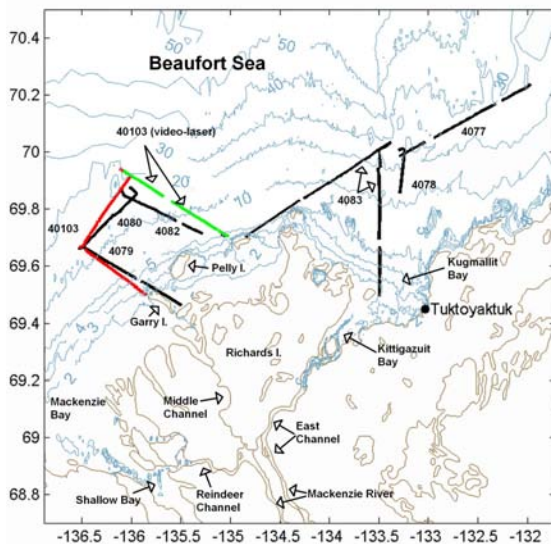


Fig. 3: Lower Mackenzie delta, showing bathymetry (blue) and IcePic survey tracks (black—Apr 26, and red—May 11). A high-altitude survey line (green) was also flown to acquire ice roughness and video.

Survey flights were conducted on Apr 26 (Lines 4077-4083) and May 11 (Line 40103) in 2004. Results from Line 4079 serve to illustrate some of the method's capabilities. This line extends from grounded ice located southeast of Garry Island, passed over three bars adjacent to the

island where the sub-ice sediments were known to be unfrozen, shallow-frozen or deeply frozen (Steven Solomon, personal communication), then into deeper water almost perpendicular to the local bathymetric contours, through the extensively ridged and rubbled stamukhi zone, and ending near the 15m contour.

## Models and Methods

Under normal Arctic offshore ice conditions, sea ice with electrical conductivities ranging from 0.05 S/m or higher for thin, new ice, down to 0.001 or lower for cold, low-salinity multi-year or freshwater ice (Morey et al., 1984), floats on seawater with conductivity of 2.5 S/m (Macdonald et al, 1992).

The large conductivity contrast between the ice and water facilitates the estimation of ice thickness using EM induction measurements in the 1 kHz to 100 kHz range, coupled with an accurate means of measuring the distance between the EM sensor and the snow/ice surface, such as an accurate laser altimeter. The relationship between EM induction amplitudes and phases and ice thickness is not linear, so it is necessary to “invert” the observed EM-Laser data using a precise forward model and a nonlinear inversion method to estimate ice thickness. If multiple frequencies of accurate data are inverted jointly, it is also possible to estimate the bulk conductivity of the ice and sub-ice water.

A “generic” airborne EM induction sea ice measurement system thus comprises an electromagnetic induction sensor operating at one or more frequencies in the range 1 kHz to 100 kHz, a laser altimeter, a GPS receiver and a real-time ice properties processor, mounted on or towed beneath an aircraft. The processing unit effectively estimates the distance between the EM sensor and the sub-ice seawater based on the strength of the EM signal arising from eddy current induction at the seawater surface, subtracts the laser-derived height of the EM sensor above the ice/snow surface, and for multi-frequency systems, estimates the upper and lower layer conductivities based on variation of the EM response with frequency.

The ice and sub-ice water conditions in the Mackenzie Delta are more complex than the “offshore” model described above (Solomon, Fraser and Manson, 2005, Solomon, Taylor and Stevens, 2008, Stevens, Moorman and Solomon, 2008). Inshore, the ice is fresh and grows down from the surface until it reaches the bottom sediments. Depending on ice thickness, water depth and other factors, the ice may bond to the bottom and initiate freeze-back of sediment. If there is permafrost at depth, then freeze-back may reach the permafrost. Frozen sediments typically display very low electrical conductivities, while unfrozen sediments containing silts and clays, particularly those that have been deposited in seawater, tend to be fairly conductive.

Mackenzie River water flows in a plume beneath the ice. Its lower density ensures that it flows along the ice bottom until it encounters obstructions such as the as large ice ridges of the stamukhi, which cause sub-ice ponding of the freshwater. Diffusion and turbulent flow along the way drive mixing, which progressively increases the salinity of this low-density water as it flows seaward along the bottom of the ice.

Under these conditions, the use of *a priori* data (conductivity of 0.001S/m for ice and freshwater), and adjusted starting model parameters permit inversion of the observed data for a two-layer model with very low upper layer conductivity and variable thickness, representing snow plus ice plus freshwater or frozen sediments where present, with a moderate, variable lower layer conductivity representing conductive sediments or saline water. Three-layer models (not shown here) yielded similar results but with “noisier” parameter estimates.

Fig. 4 below describes in schematic form the ice and water conditions observed along survey line 4079 (see line location in Fig 3.) This profile links a series of zones in which particular combinations of ice and water properties were present, as interpreted from the multi-frequency EM/Laser data and in some cases corroborated by Envisat Advanced Synthetic Aperture Radar (SAR or ASAR) imagery.

In Zone I, above the 2m bathymetric contour, ice formed from fresh Mackenzie River water directly overlies deeply frozen (Zone IA); shallow-frozen (Zone IB); and unfrozen (Zone IC) sediments, with the possible presence of a thin layer of freshwater at high tide. The electrical conductivities of freshwater ice and frozen sediment are comparable, making these materials indistinguishable to the EM measurements. A strong contrast in conductivity at the depth where unfrozen sediments were present beneath ice and frozen sediments, perhaps associated with brine migration during freeze-back, permits this interface to be profiled.

In Zone II (also see Fig. 7 below), between the 2 and 7m depth contours, a freshwater plume of river water underlies the ice, ponded behind the thick ice of the stamukhi. In this interval, the combined ice and freshwater thickness should match the observed bathymetry.

In Zone III, beyond 7m depth, a layer of seawater underlay the freshwater plume, which would cause an increase in the average conductivity at depth and a decrease in the apparent thickness of the ice plus freshwater layer. The cartoon represents the ridges of the stamukhi in Zones III and IV by their minimum keel drafts, since it is these minima that control the ponding depth of freshwater. Grounding of these ridge and rubble features is likely along their lengths.

In Zone IV, between bands of ridged and rubbled ice in the stamukhi, ponded zones of progressively higher salinity water trend toward normal sea ice overlying seawater beyond the 20m depth contour.

## RESULTS

In Fig. 5, the upper layer thickness (solid black) was plotted with a bathymetric profile (magenta dashed) obtained by a nearest-neighbor method from digital field sheets 1300872 and 1300962, acquired during Canadian Hydrographic Service (CHS) acoustic sounding surveys conducted in 1971 and 1974, corrected to account for tidal variation at the time of the survey and for nominal ice freeboard. It should be noted that these bathymetric data are almost 40 years old, and may be expected to exhibit some inaccuracies due to coastal erosion and aggradation since their acquisition, particularly in shallow areas (Solomon, Fraser and Manson, 2005). Ice and frozen sediment conductivities were assumed to be very low (0.001 S/m), and unfrozen sediment was assumed to have conductivity 0.3 S/m, based on EM data fitting and consistent with previous estimates for unfrozen sediments (Scott, 1994). The two areas where the upper layer thickness exceeds 6m appear to represent two zones of ice-bonded, deeply frozen sediment, which coincide with shallow bathymetry as indicated. An auger measurement, obtained on an opportunity basis near the beginning of this survey line and apparently in Zone IC or II conditions, indicated a total snow plus ice thickness of 1.70m, with freshwater present beneath the ice. A bathymetric estimate was not obtained at this site. Additional augered ice thickness estimates could not be established during these flights due to time and fuel constraints.

The inversion results in Fig. 6 indicate that, from 190 to 220 seconds, the EM-estimated upper layer thickness, ranges from 0 to 0.8m thicker than the nearby augered snow plus ice thickness measurement. The upper layer thickness is also approximately equal to the bathymetry. This implies that the ice, plus a 0 to 0.8m layer of freshwater, overlies conductive, unfrozen sediment.

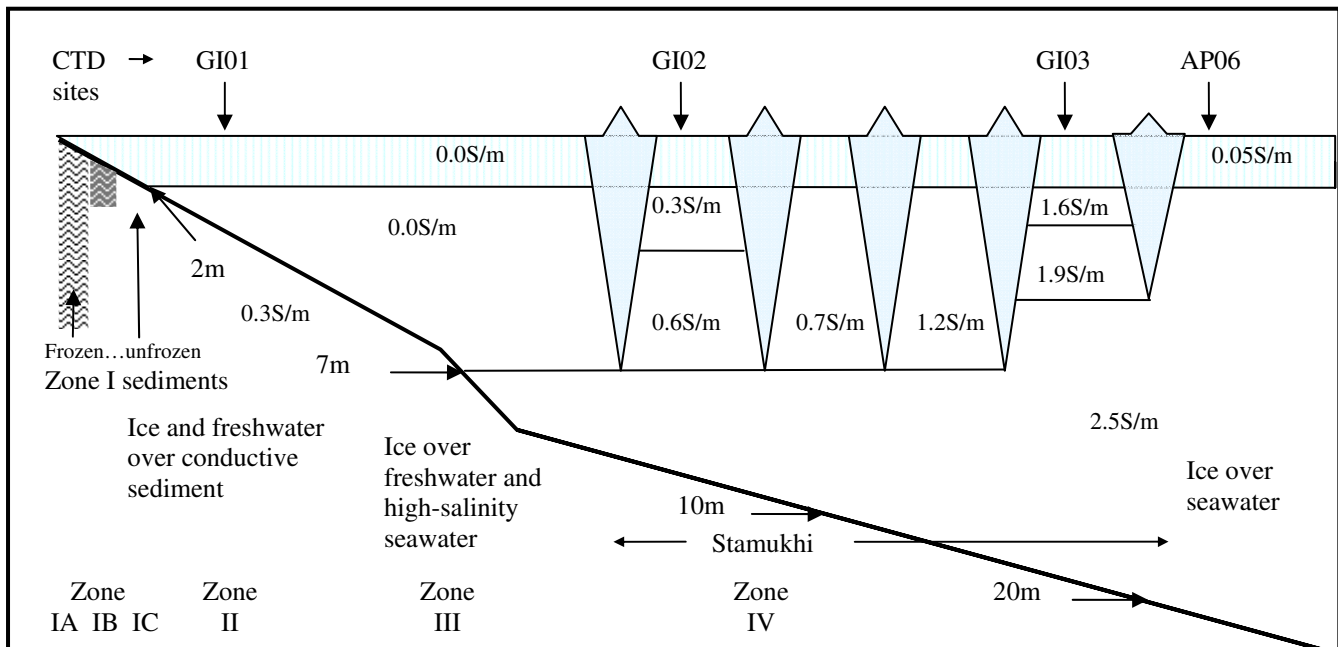


Fig. 4: A cartoon showing the range of conditions encountered along line 4079 as a cross section, extended into offshore pack ice conditions. CTD profile sites are shown schematically at top. The zones listed at bottom are described in the text. The light blue features represent flat-lying ice, while the quasi-triangular shapes represent the minimum draft of ice and rubble features. A heavy diagonal black line shows the interface between ice or water and bottom sediments. Bathymetric contours are indicated along this line by short horizontal arrows. Hatched areas represent frozen sediments.

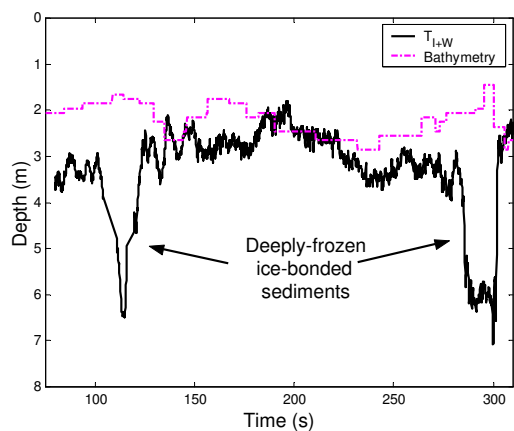


Fig 5: Profile of inverted upper layer thickness (solid black), plotted with CHS bathymetry (dashed magenta), indicating two known areas of Zone IA ice-bonded permafrost at which surficial ice overlies deeply frozen sediments, centered at 110 and 290 seconds. Note shallower bathymetry at these locations, corresponding to diagnostic SAR image features indicating the presence of ice-bonded frozen sediments (see Fig 9 below). This extract is approximately 9 km long.

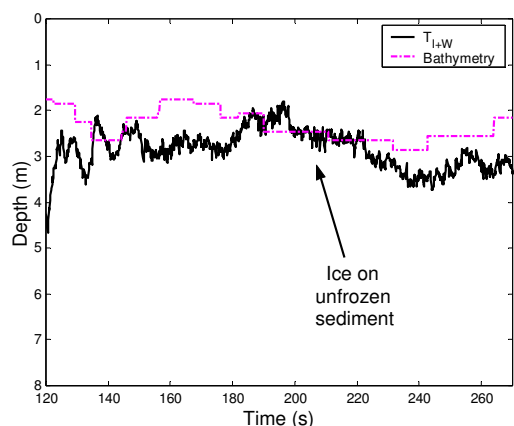


Fig. 6: Profile of inverted upper layer thickness (black) plotted with CHS bathymetric data (dashed magenta). Annotation indicates the location of Zone IC conditions, where ice and a thin layer of fresh water overlie unfrozen sediments between 180 and 220 seconds. Two areas of Zone IB shallow-frozen ice bonded sediments at 170 and 240 seconds, for which the upper layer thickness substantially exceeds the bathymetry, are also visible. This extract is approximately 6 km long.

The Zone II profile in Fig 7 compares the upper layer thickness, corresponding to ice plus freshwater, with the observed bathymetry along this section of the line. A similar technique could be used with IcePic data to obtain bathymetric profiles for ice-covered lakes and rivers in which relatively low conductivity ice and freshwater overlie high conductivity sediments such as clays.

Under the right conditions, a related approach can be used to estimate the thickness of seawater beneath ice over a resistive bottom. This method was first demonstrated by Kovacs and Holladay (1990) near Prudhoe Bay, USA, and used operationally by the Canadian Hydrographic Service TIBS airborne electromagnetic system to chart bathymetry in portions of Pelly Bay and Coronation Gulf, Canada.

CTD profiles and acoustic spot sounding data were used to provide the *a priori* inversion constraints for those surveys. While the IcePic was not designed to acquire approximate bathymetric data in seawater beneath ice, it could be used for this purpose in shallow waters, if suitable *a priori* inputs were available.

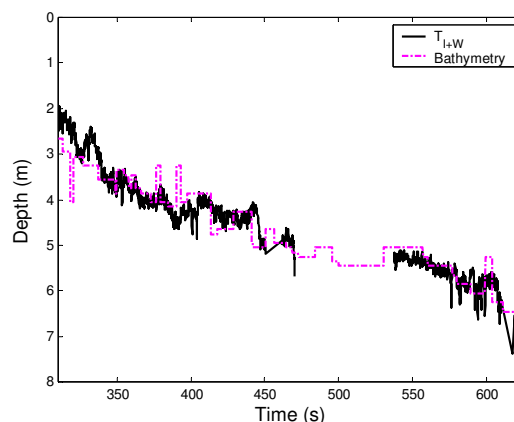


Fig. 7: Ice plus freshwater depths closely match CHS-measured bathymetry in this 12 km profile extract, where ice overlies freshwater over conductive sediment, corresponding to Zone II in Fig. 4.

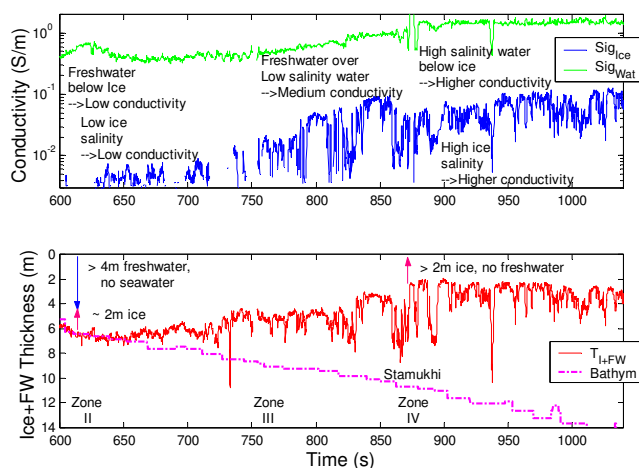


Fig. 8: Profiles of upper layer conductivity (blue), thickness (red) and lower-layer conductivity (green), plotted with CHS bathymetry for Zones II to IV. This profile extract is approximately 17 km long.

In Fig. 8, the upper and lower layer thickness and conductivity profiles are color coded for consistency with the next two figures. In Zone II, ice and sub-ice water comprising the upper layer are fresh and display low conductivities ( $\sim 0.001$  S/m), while the bottom sediments comprising the lower layer have moderate conductivities in the 0.3 S/m range. Where these assumptions are valid, model-based sensitivity analysis suggests that upper layer thickness accuracy should be on the order of 0.01m or better for level ice, while conductivity accuracies should be on the order of 0.001 S/m. Such estimates are based on idealized assumptions and typically overestimate achievable accuracies. Both upper and lower layer conductivities are higher in Zone III, due to the presence of freshwater overlying low-salinity water beneath the ice, while the upper layer's apparent thickness decreases as an increasing proportion of high-salinity water is included in the lower layer.

In the stamukhi (Zones III and IV), bands of ridged ice roughly parallel to shore impede seaward freshwater flow, causing ponding of low-density fresh and low-salinity water beneath the ice. Progressive mixing increases the salinity of sub-ice waters and the ice itself toward the outer edge of the stamukhi. In deep water (not shown in this profile), normal (2m thick, 0.05 S/m) sea ice overlies normal seawater.

The composite plot in Fig. 9 incorporates enhanced satellite ENVISAT SAR data (Solomon, Fraser and Manson, 2005), the EM system's flight path, and the inverted upper layer thickness and lower layer conductivity along this line. Both the HH and HV channels were enhanced with a simple linear stretch, with HH, HH and HV displayed as red, green and blue.

ENVISAT ASAR APP HH+HV IS7: 29 Apr 2004 (0639Z) RGB=HH,HH,HV  
FEM T1+S2: 26 Apr 2004: FEM04079PPR.IPP

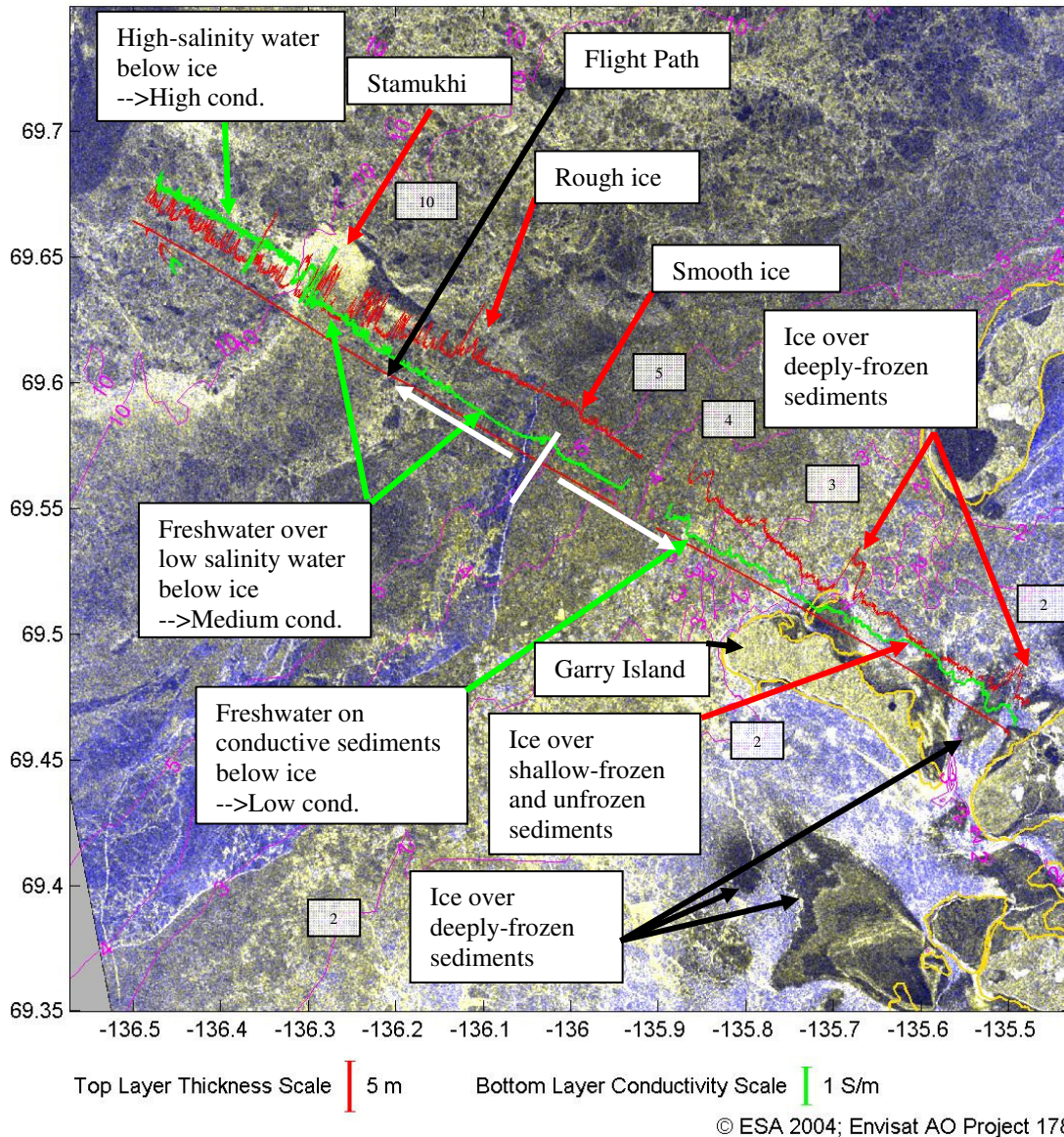


Fig. 9: Detail of two-layer EM model results (upper layer thickness in red, basal layer conductivity in green) and bathymetric contours (violet, depth labels in metres added in white boxes) for Line 4079, superimposed on enhanced HH+HV polarization ENVISAT SAR imagery from April 29, 2004. The profile data, acquired on April 26, 2004, are plotted relative to the flight path (smooth red line). Note jump in basal conductivity at 10m contour.

Starting at the inshore end of the survey line (right side of figure, southeast of Garry Island), note the zones of very smooth ice, indicated in the enhanced SAR image by dark grey or black areas, which overlie ice-bonded permafrost and correspond to Zone 1A in Fig. 4. Contrasting with these permafrost areas are transitional regions (mottled white and blue in SAR image) where ice and very shallow freshwater overlie unfrozen sediment, corresponding to Zone 1C in Fig. 4. As previously seen in Figs. 5 and 6, the inverted upper layer

thickness shows strong peaks over the Zone 1A ice-bonded permafrost, with a relatively smooth profile between them corresponding to shallow-frozen sediments (Zone 1B) and ice plus a thin freshwater layer overlying unfrozen (Zone 1C).

Farther to the northwest, the landfast ice becomes smoother over Zone II ice plus freshwater overlying sediments. The transition to Zone III ice and freshwater floating on more saline water is annotated with a

white bar perpendicular to the flight path, located in relatively smooth ice bordering a refrozen flaw lead, while the stamukhi is marked by ridging in the profile and light, bright colors in the SAR image. A jump in basal conductivity occurs at a bright ridge at the 10m bathymetric contour in the stamukhi zone.

The profile ends near a large, smooth refrozen flaw lead (dark blue) near the outer edge of the stamukhi. The enhanced SAR and reprocessed EM results are seen to yield consistent and complementary data for the entire survey line.

ENVISAT ASAR APP VV+VH IS6: 26 Apr 2004 (0633Z) RGB=VV,VV,VH  
 FEM T1+S2: 11 May 2004: FEM04103PPR.IPP  
 Video/Laser Ice Roughness: 11 May 2004

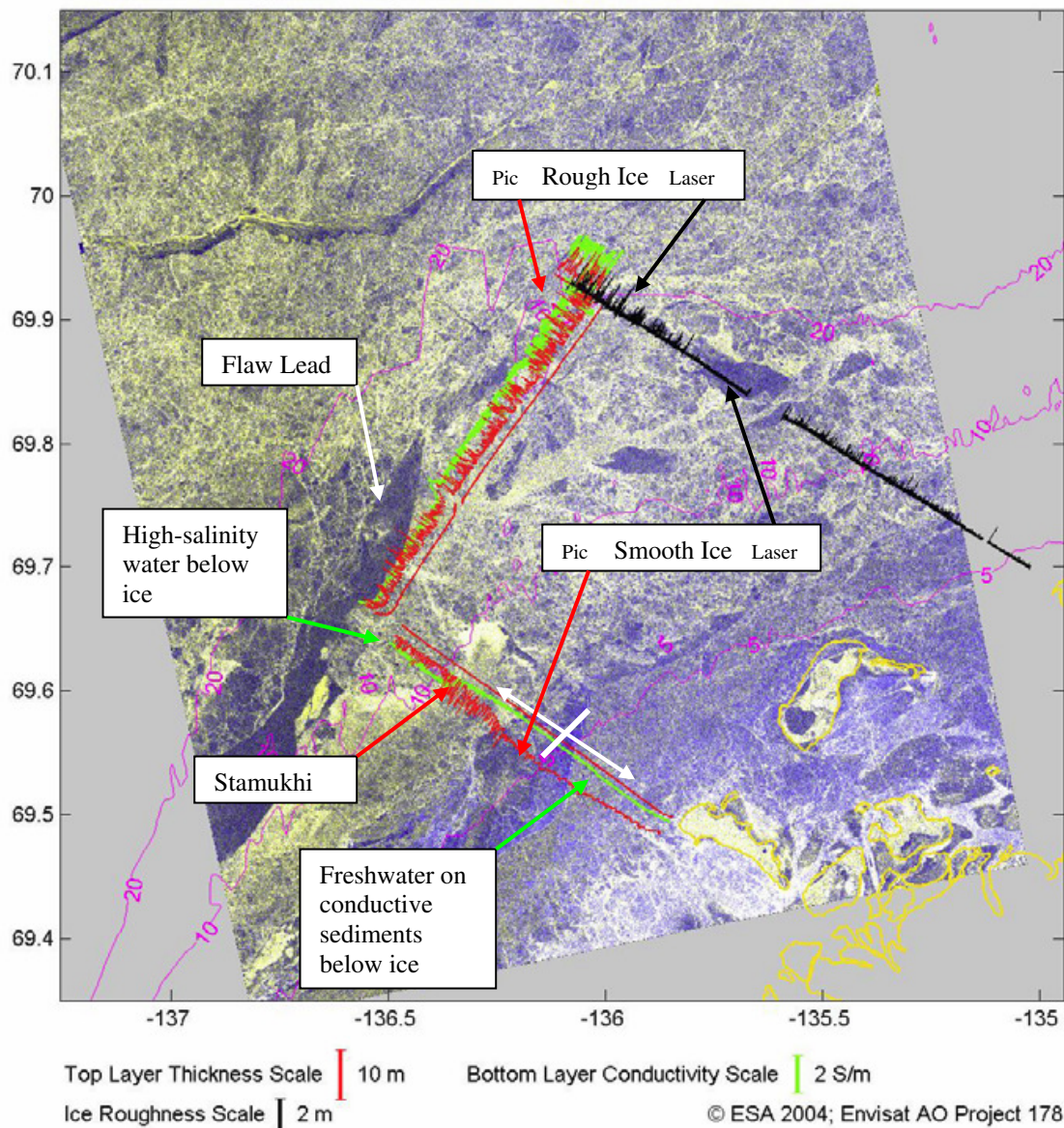


Fig. 10 These profiles were acquired on May 11, almost three weeks after those shown in Fig. 9. The same color scheme was used to plot the IcePic data, with the addition of the laser-estimated ice roughness profile shown in black at upper right. The enhanced ENVISAT SAR image used as an underlay is from 26 April, and used VV+VH polarizations. A jump in basal conductivity again occurs at strong ridging near the 10m contour.

A second IcePic dataset over this area was acquired on May 11. The reprocessed results from this flight were overlaid onto an April 26 Envisat SAR image that was acquired using different polarizations and enhancements. Zones of ice-bonded sediments are still visible, though rendered slightly differently than in the previous example, and the May 11 survey line does not cross regions of ice-bonded frozen sediments. Note that the layer thickness and lower layer conductivity profiles were

plotted with a reversed plotting sense in this example relative to the previous figure. This profile runs to the NW, slightly to the south of the previous profile, then turns and extends to the NNE. Zone II, III and IV conditions were encountered by the first leg of this profile, while the second leg runs through rough ice and increasing lower-layer conductivity corresponding to Zone IV increasing water conductivity, roughly parallel to the outer edge of the stamukhi. The black trace

running to the southeast (note color-coded scale at bottom of figure) shows the correspondence of the surface roughness, as sensed by the system's laser altimeter, to the roughness visible in the SAR image.

## CONCLUSIONS

Examples from a 2004 IcePic survey in the Mackenzie Delta illustrate ways in which the standard processing methods used for real-time EM ice thickness measurement can be augmented through in-field post-processing using limited *a priori* constraints to yield:

1. estimates of bulk ice conductivity that can help to distinguish freshwater ice from normal sea ice,
2. estimates of sub-ice water conductivities,
3. identification and mapping of sub-ice freshwater plumes dammed behind ice ridges,
4. estimation of ice plus freshwater layer thickness over conductive sediments (approximate bathymetry) or saline water, and
5. discrimination between ice lying on unfrozen sediments and ice bonded to deeply frozen sediments (permafrost).

The first four capabilities have proven useful for winter studies in the Mackenzie Delta, and are likely to find application in understanding sub-ice conditions in other Arctic and subarctic bays and estuaries, particularly where river discharges form coherent sub-ice plumes. The ability to map ice-bonded sediments using airborne methods should be useful for studies of permafrost formation and degradation, providing a way to rapidly survey relatively large areas as a bridge between satellite SAR interpretation and highly detailed, surface based radar and borehole observations. Further survey work is planned in the area in coordination with a surface measurement program.

## ACKNOWLEDGEMENTS

The authors gratefully acknowledge information, insights, suggestions, data and graphics provided by Steven Solomon. Field data acquisition was greatly facilitated by CCGS Amundsen Captain Bernard Tremblay, with flight support by helicopter pilot Yvon Coté and helicopter engineer Bertrand Murray. ENVISAT SAR data were provided by the European Space Agency under AO Project 178. Financial support was provided by CASES (L. Fortier and D. Barber), through the Can. Space Agency-GRIP program, the Panel of Energy and Research Development and through Geo. Service Canada Atlantic Region (G. Mason) and Devon Oil Canada (D. Scott and B. Wright).

## REFERENCES

ACIA (2004). Impacts of a Warming Arctic: Arctic Climate Impact Assessment. Cambridge University Press.

ACIA (2005) Arctic Climate Impact Assessment. Cambridge University Press, 1042p.

Mackenzie Delta Field Sheet 1300872 (1971). Canadian Hydrographic Service, Burlington, Ontario, Canada.

Mackenzie Delta Field Sheet 1300962 (1974). Canadian Hydrographic Service, Burlington, Ontario, Canada.

Haas, C., Hendricks, S., Doble, M. (2006), Comparison of the sea ice thickness distribution in the Lincoln Sea and adjacent Arctic Ocean in 2004 and 2005, *Annals of Glaciology*, 44, 247-252.

IPCC (2007): Climate Change 2007: The Physical Science Basis. Contribution of Working Group I to the Fourth Assessment

Report of the Intergovernmental Panel on Climate Change [Solomon, S., D. Qin, M. Manning, Z. Chen, M. Marquis, K.B. Averyt, M. Tignor and H.L. Miller (eds.)]. Cambridge University Press, Cambridge, United Kingdom and New York, NY, USA, 996 pp.

Kovacs, A. and Holladay, J.S. (1990). Sea ice thickness measurement using a small airborne electromagnetic sounding system, *Geophysics* 55, 1327-1337

Kovacs, A, Holladay, J.S., and Bergeron, C (1995). The footprint/altitude ratio for helicopter sounding of sea-ice thickness: Comparison of theoretical and field estimates, *Geophysics* 60, 374-380.

Macdonald, R.W. and E.C. Carmack (1991). The role of large-scale under-ice topography in separating estuary and ocean on an Arctic shelf. *Atmosphere-Ocean* 29:37-53.

Macdonald, R.W., R. Pearson, D. Sieberg, F.A. McLaughlin, M.C. O'Brien, D.W. Paton, E.C. Carmack, J.R. Forbes, J.Barwell-Clarke (1992). NOGAP B.6, Physical and chemical data collected in the Beaufort Sea and Mackenzie River delta, April-May 1991, *Can. Data Rep. Hydrogr. Ocean Sci.*: 104, 154 pp.

Macdonald, R.W., D.W. Paton and E.C. Carmack (1995). The freshwater budget and under-ice spreading of Mackenzie River in the Canadian Beaufort Sea based on salinity and 18O/16O measurements in water and ice. *Journal of Geophysical Research* 100(C1): 895-919.

Melling, H., D. A. Riedel, and Z. Gedalof (2005). Trends in the draft and extent of seasonal pack ice, Canadian Beaufort Sea, *Geophys. Res. Lett.*, 32, L24501, doi:10.1029/2005GL024483.

Morey, R.M., A. Kovacs, and G. F. N. Cox (1984). Electromagnetic properties of sea ice: *Cold Regions Science and Technology*, 9, 53-75.

Peterson, I. K., S. J. Prinsenberg, and J. S. Holladay (2008). Observations of sea ice thickness, surface roughness and ice motion in Amundsen Gulf, *J. Geophys. Res.*, 113, C06016, doi:10.1029/2007JC004456.

Prinsenberg, S. J., S. Holladay, and J. Lee (2002). Measuring Ice Thickness with EISFlow™, a Fixed-mounted Helicopter Electromagnetic-laser System, Proceedings of the Twelfth (2002) International Offshore and Polar Engineering Conference, Kitakyushu, Japan, May 26-May 31, 2002, Vol. 1, pp. 737-740

Prinsenberg, S. J., I. K. Peterson, and S. Holladay (1996). "Comparison of Airborne Electromagnetic Ice Thickness Data with NOAA/AVHRR and ERS-1/SAR Images". *Atmos.-Ocean*, 34(1), pp. 185-205.

Rossiter, J.R., J.S. Holladay and L.A. Lalumiere (1992). Validation of airborne sea ice thickness measurement using electromagnetic induction during LIMEX '89, *Can. Contractor Rep. Hydrog. And Ocean Sci.* 41.

Scott, W.J. (1994). Inversion of EM Profiles, Mackenzie Delta Area, NWT, Report under SSC Contract 23420-01M465/001/HAL, prepared for S. Solomon by GeoScott Exploration Consultants Inc.

Solomon, S.M, P. Fraser, G.K., Manson (2005). Nearshore morphology derived from synthetic aperture radar in the Mackenzie Delta region of the Beaufort Sea, *Proc. Can. Coastal Conf.* 2005.

Solomon, S.M, A.E. Taylor, C.W. Stevens (2008) Nearshore ground temperatures, seasonal ice bonding, and permafrost formation within the bottom-fast ice zone, Mackenzie Delta, NWT, *Proc Ninth Int. Conf. on Permafrost*.

Stevens, C.W., B.J. Moorman, S.M. Solomon (2008). Detection of Frozen and unfrozen interfaces with ground penetrating radar in the nearshore zone of the Mackenzie Delta, Canada, *Proc Ninth Int. Conf. on Permafrost*.

Wadhams, P., and N. R. Davis (2000). Further evidence of ice thinning in the Arctic Ocean, *Geophys. Res. Lett.*, 27(24), 3973-3975.